Measurement of mineral elastic modulus through nanoindentation

By

Pu Deng

A thesis submitted to the Graduate Faculty of
Auburn University
in partial fulfillment of the
requirements for the Degree of
Master of Science

Auburn, Alabama
May 6, 2017

Keywords: Nanoindentation, mineral, elastic modulus, thin film

Approved by

Barton Prorok, Chair, Professor of Materials Engineering
Dong-Joo Kim, Professor of Materials Engineering
Ruel A. Overfelt, Professor of Materials Engineering

Abstract

Minerals are the main component of Earth's crust and mantle. For our planet, the data we have on the Earth's interior are obtained from the measurement of seismic wave velocity. Measurement in laboratory of mineral's elastic properties are vital for the understanding of seismic information. The method we used here to determine mechanical properties of mineral is nanoindetation also called depth sensing indentation (DSI). DSI is a reliable and fast testing method to determine mechanical properties of materials, it relies on the relationship between elastic modulus and loading and unloading displacement data. Conventional DSI is directly indent on mineral surface which may cause the form of crack owing to high stress concentration caused by indenter tip. The unloading slope is called stiffness which describe the extent to resist deformation, formed crack and defects would lower the stiffness compared to expected value and lead to smaller elastic modulus. In order to eliminate the effect of crack and other defects, a chromium film is deposited on mineral sample. The elastic modulus of mineral can be obtained without penetrating into it, since the set penetration depth would be the thickness of deposited film. This is started from the model developed by Bo Zhou and Bart Prorok, which could be used to deal with film substrate

system, and method developed by Yan Chen and Bart Prorok, which shows good results for measuring modulus for brittle material. Minerals are chosen for samples due to its representativeness of brittle material and inaccurate modulus results measured so far. Scanning Electron Microscope (SEM) was used to determine film thickness after deposited, Z-P model and Chen-Prorok method was employed to obtain substrate modulus form raw data.

Acknowledgments

I would like to thank Dr.Prorok, my advisor, for his guidance and support. I would like to thank Yan Chen and Anqi Zhang, who gave me a lot of help during this work. And my partner, Sean Vincent Herrera, thanks for his efforts during this work. Thanks for SEM training from Steven Moore and magnetic sputter training from Eunji Lee.

Table of Contents

Abstract ii

Acknowledgments iii

List of Tables vi

List of Figures vii

Chapter 1 INTRODUCTION 1

1.1 Nanoindentation 1

1.2 Continuous stiffness measurement (CSM) 4

1.3 Film-substrate composite system 5

1.4 Zhou-Prorok model 6

1.5 Chen-Prorok method 7

Chapter 2 SAMPLES and METHODS 10

2.1 Mineral sample 10

2.2 Sample preparation 11

2.3 Experiment 14

Chapter 3 RESULTS and DISCUSSION 19

3.1 Indentation data and SEM images 19

3.2 Pop in 32

3.3 Zhou-Prorok model and Chen-Prorok method results 34

Chapter 4 CONCLUSIONS 38

References 39

List of Tables

Table 1 Crystal system and formula of sample 11

Table 2 Chromium deposition parameters 14

Table 3 Film thickness measurement and X-Ray Diffraction result 16

Table 4 Substrate information and calculated results for all minerals 34

List of Figures

Figure 1.1 A schematic representation of load versus displacement for an indentation experiment [1] 1

Figure 1.2 A schematic representation of indent section for loading and unloading [2] 2

Figure 1.3 SEM images for different indent impression: a) sink in b) normal c) pile up [5] 4

Figure 1.4 A schematic representation of CSM model [6] 5

Figure 1.5 Elastic modulus versus displacement for an amorphous near-frictionless carbon film [11] 6

Figure 1.6 Comparing Zhou-Porork model with Doerner-Nix model and Gao model [11] 7

Figure 1.7 A schematic representation of function I and its asymptote I' [16] 9

Figure 2.1 Ten chosen mineral samples for this work 10

Figure 2.2 Struers Accutom-5 cutting machine 12

Figure 2.3 Struers RotoPol-11 Surface Polisher 12

Figure 2.4 Denton Discovery 18 sputtering system 13

Figure 2.5 JEOL JSM 7000F scanning electron microscope..... 15

Figure 2.6 SEM image for film thickness measurement..... 15

Figure 2.7 Figure 2.7 X-ray diffraction results for (a)dolomite (polycrystalline) (b)kyanite (singe crystal) (c) obsidian (amorphous) 17

Figure 3.1 A illustration of indentation test area (A) direct indentation test (B) indirect indentation test 19

Figure 3.2 Quartz indentation test and SEM images result for direct and indirect measurement 20

Figure 3.3 Obsidian indentation test and SEM images result for direct and indirect measurement 21

Figure 3.4 Beryl indentation test and SEM images result for direct and indirect measurement 22

Figure 3.5 Kyanite indentation test and SEM images result for direct and indirect measurement. 23

Figure 3.6 Dolomite indentation test and SEM images result for direct and indirect measurement 24

Figure 3.7 Microcline indentation test and SEM images result for direct and indirect measurement 25

Figure 3.8 Feldspar orthoclase indentation test and SEM images result for direct and indirect measurement 26

Figure 3.9 Calcite indentation test and SEM images result for direct and indirect measurement 27

Figure 3.10 Galena indentation test and SEM images result for direct and indirect measurement 28

Figure 3.11 Indentation test for different penetration depth on chromium-kyanite composite system (a)200nm (b)300nm (c)400nm (d)500nm 30

Figure 3.12 SEM images for particles on chromium with microcline 31

Figure 3.13 SEM image of microcline surface 31

Figure 3.14 Pop-in observed in indentation test for kyanite (a) single pop-in (b) successive pop-in 32

Figure 3.15 Load versus displacement for indirect indentation test on chromium with kyanite 33

Figure 3.16 $I(h')$ and $I(h')$ function with chromium film for different substrate Poisson's ratio [15] 35

Figure 3.17 Indentation test result, Zhou-Prorok model, L(h') function of (a) Calcite and (b)Dolomite 36

Figure 3.18 Chen-Prorok method results of (a) Calcite and (b)Dolomite 37

Chapter 1

INTRODUCTION

1.1 Nanoindentation

1.1.1 Overview

Elastic and plastic properties of small volume materials can be obtained by nanoindentation, also called depth sensing indentation, which is one of the easiest and widely used way to determine the mechanical properties of materials. Experimental results we used here is done by Nanoindenter. The indenter tip we used in this work is Bervoich tip which is three sided pyramid and geometrically self similar. Indenter tip is loaded on the sample and controlled load with corresponding displacement are recorded as shown in figure 1.1,

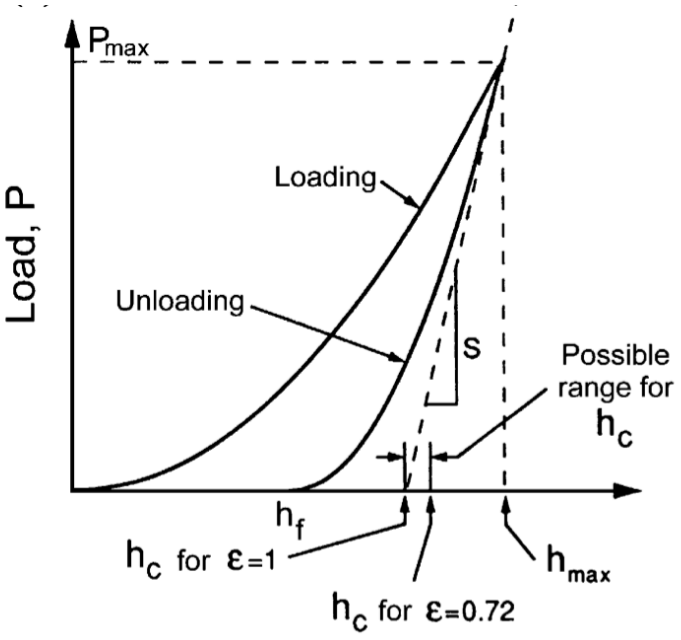

Figure 1.1 A schematic representation of load versus displacement for an indentation experiment [1].

where h_{max} is the displacement at maximum load P_{max}, h_f is final displacement after unloading, h_c is contact depth which represents the real contact area between indenter tip and sample under load. Oliver-Pharr analysis [2] is commonly used for nanoindentation, based on their analysis, elastic modulus and hardness can be obtained from the loading curve and unloading curve in figure.

1.1.2 Hardness

Hardness, which shows the extent of resistance to permanent shape change, is determine by equation:

$$H = \frac{P_{max}}{A} \quad (1)$$

where P_{max} is the maximum indentation load, A is the contact area of the hardness impression. Based on Oliver-Pharr analysis, projected contact area can be determined by contact depth as shown in figure 1.2,

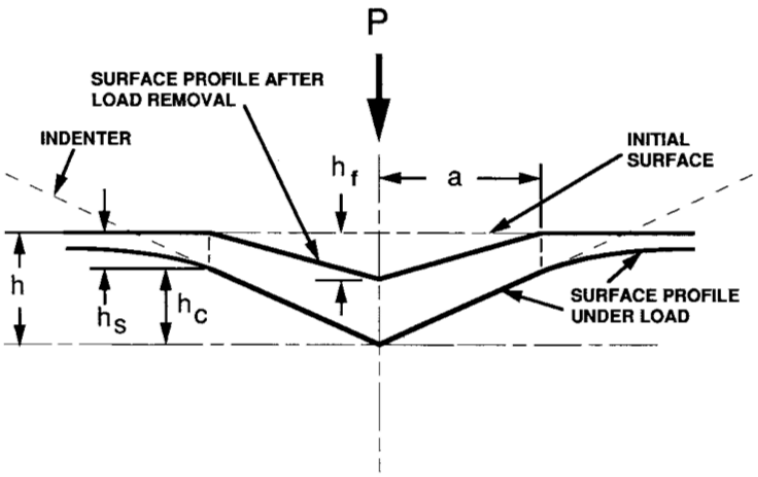

Figure 1.2 A schematic representation of indent section for loading and unloading [2].

where h, h_f and h_c are the same parameter in figure, h_s is the displacement of surface around the contact and a is the radius of contact area. For perfect Bervoich tip, the relationship between projected contact area and contact depth is:

$$A(h_c) = 24.5\ h_c^2 \quad (2)$$

However, in real situation, the indenter tip is not perfect sharp, the calibration for tip blunting is required. Calibrated tip area function is show below:

$$A(h_c) = 24.5\ h_c^2 + C_1\ h_c^1 + C_2\ h_c^{1/2} + C_3\ h_c^{1/4} + \ldots\ldots + C_8\ h_c^{1/128} \quad (3)$$

where C1 through C8 are constants.

1.1.3 Elastic modulus

Sneddon [3] derived the equation for elastic modulus which is independent of indenter tip geometry, as shown below:

$$E_r = \frac{\sqrt{\pi}}{2\beta} \frac{S}{\sqrt{A(h_c)}} \qquad (4)$$

where β is a dimensionless indenter shape constant ($\beta_{berkovich} = 1.034$) and it is used to account for deviations in stiffness due to the asymmetry of axial for pyramidal indenters, E_r is reduced modulus, which is defined to describe elastic the deformation for both indenter tip and sample under load. E_r is given by

$$\frac{1}{E_r} = \frac{(1-\nu^2)}{E} + \frac{(1-\nu_i^2)}{E_i} \qquad (5)$$

where ν and ν_i are Poisson's ratio of specimen and indenter tip, E and E_i are elastic modulus of sample and indenter tip. For Bervoich tip, which is made of diamond, the E_i and ν_i is 1141GPa and 0.07 [2], respectively. S refer to stiffness, which is the slope the unloading curve at upper portion, and is defined by:

$$S = \frac{dP}{dh} \qquad (6)$$

After the parameter such as contact area, stiffness and contact depth are obtained based on the load-displacement curve and equation, elastic modulus can be calculated.

1.1.4 Deficiency

The most important deficiency of Oliver-Pharr analysis is it can not account for pile up and sink in [4]. For pile up, which is indented material move onto the surface plane, underestimation of contact area occurs and lead to overestimation of hardness and elastic modulus. This happens when indenter tip penetrates into soft material. In turn, sink in happens when indent on hard material. Similar effect occurs when the sample is film-substrate composite, sink in occurs if the substrate is more compliant than film, pile up occurs if the substrate is more stiff than film. Schematic representation of pile up and sink in is shown in figure 1.3,

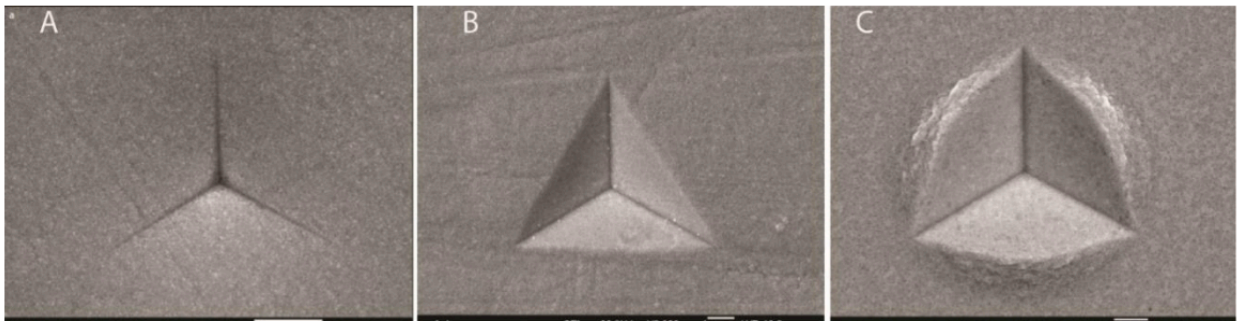

Figure 1.3 SEM images for different indent impression: a) sink in b) normal c) pile up [5]

where Figure a shows sink in, Figure b shows normal indent impression and Figure c shows pile up. Most of test results are suffering from sink in, because for film-substrate system, almost all minerals we used in this work are more compliant than chromium, and for bulk material, minerals are treated as hard materials.

1.2 Continuous stiffness measurement (CSM)

The measurement of nanoindentation is highly improved and facilitated by a technique called continuous stiffness measurement. As explained above, traditional way to determine stiffness is by calculating the slope of unloading curve. For continuous stiffness measurement, as the name implies, the stiffness is measured continuously during the loading, which is accomplished by imposing a harmonic force, shown in figure 1.4.

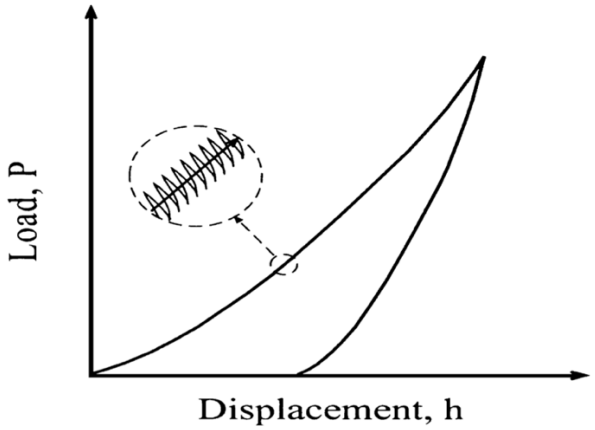

Figure 1.4 A schematic representation of CSM model [6]

Stiffness can be calculated from imposed harmonic force and response displacement of indenter. This technique provides continuous results of stiffness versus displacement and significantly reduces the calibration time. All indentation results we used in this work in obtained under CSM model.

1.3 Film-substrate composite system

After depositing metallic film on mineral samples, monolithic sample changes to film-substrate composite system. The behavior of monolithic sample and composite system are different under nanoindentation test. Oliver-Pharr analysis is primarily developed for monolithic materials and it can not obtain accurate result when applied to film substrate system. Since when indenter tip punched into film, the response is the mixture of film and substrate and this will complicate the result. This is a well-known phenomenon called substrate effect [7-9]. For instance, pile-up and sink-in, as introduced before, both will lead to inaccurate results.

There is a rule a thumb came from Buckle [10] suggest that a relatively substrate independent and accurate result can be obtained if the penetration depth is within 10% of film thickness. As shown in figure 1.5,

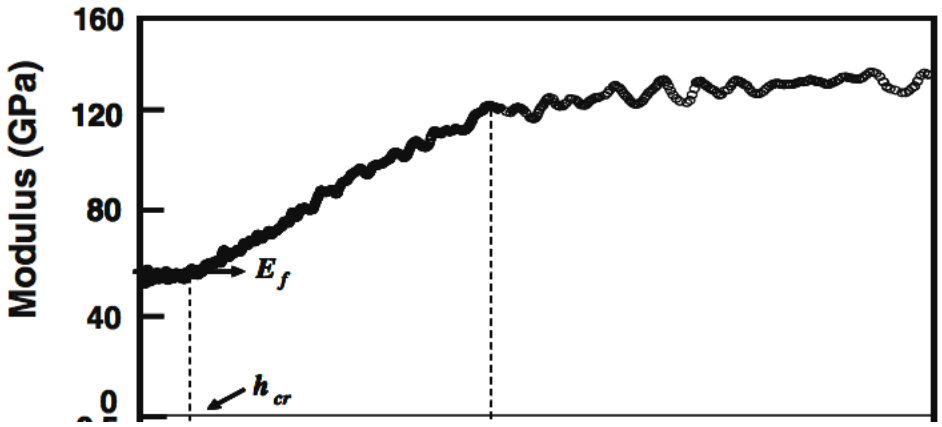

Figure 1.5 Elastic modulus versus displacement for an amorphous near-frictionless carbon film [11]

it is clear that at small displacement, the modulus appears to be constant and the penetration depth approaching film substrate, the influence of substrate is increasing. However, in some cases, the film thickness is very small, at this scale, accurate results can not be obtained. Moreover, in this work, the desired results are the elastic modulus of substrate, hence, different approach will be introduced.

1.4 Zhou-Prorok model

In order to describe the behavior of film substrate composite system, a variety of models and equations have been developed. Doerner and Nix [12] first introduced a weighting factor and derived an empirical function to describe the contribution of film and substrate. Gao and co-workers analyzed composite system by moduli-perturbation method and derive a solution and

introduce some parameters. The model we used here is Zhou-Prorok model [13] which is developed by Bo Zhou and Bart Prorok because it shows better performance for extracting substrate modulus from composite system than Doerner-Nix model and Gao model [14]. As shown in figure 1.6:

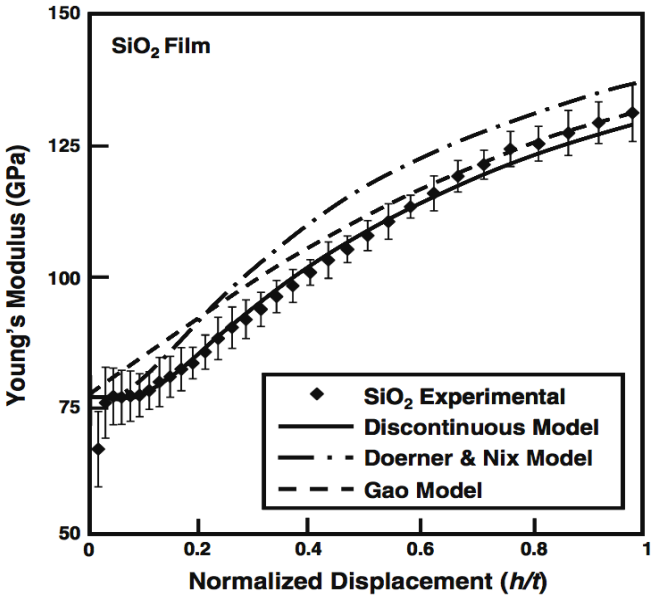

Figure 1.6 Comparing Zhou-Porork model with Doerner-Nix model and Gao model [11].

where h/t is normalized displacement, t is film thickness. The basic form of Zhou-Prorok model is:

$$\frac{1}{E_t} = \frac{1}{E_f}(1 - \Phi_s) \cdot \left(\frac{E_f}{E_s}\right)^{0.1} + \frac{1}{E_s}\Phi_f \qquad (8)$$

where E_t is composited modulus, tested from indenter, E_f and E_s are film modulus and substrate modulus, Φ_s and Φ_f are weighting factor, $\Phi_f = e^{-\nu_f(t/h)}$, $\Phi_s = e^{-\nu_s(t/h)}$, where ν_f and ν_s are film Poisson's ratio and substrate Poisson's ratio, t is film thickness and h is penetration depth. By employed this model, substrate modulus could be extracted from composite modulus if E_f, ν_f and ν_s are known.

1.5 Chen-Prorok method

In order to extract substrate modulus from composite system by employing Zhou-Prorok model, we have to preknow the film thickness and material properties including Poisson's ratio and elastic

modulus. The value of this variables either need to be measured in laboratories like film thickness or we have to search for literature value which may not be exactly correct like Poisson's ratio and modulus. Chen-Prorok method [15] is a more general method to extract substrate modulus from composite system. This method is derived by rearrange Zhou-Prorok model:

$$\frac{1}{E_t}\ \frac{1}{\left(1-\mathrm{e}^{-\nu_s/h'}\right)} = \frac{1}{E_f'} + \frac{1}{E_s}\frac{e^{-\nu_f/h'}}{\left(1-\mathrm{e}^{-\nu_s/h'}\right)} \qquad (9)$$

where h' is termed reduced displacement and equals to h/t, another term is simplified:

$$\frac{1}{E_f'} = \frac{1}{E_f}\left(\frac{E_f'}{E_s'}\right)^{0.1} \qquad (10)$$

The most impressive transformation of this equation is it convert weighting factor part, which is $\frac{e^{-\nu_f/h'}}{\left(1-\mathrm{e}^{-\nu_s/h'}\right)}$ and refer to as I(h′), to a linear approximation, which is $0.5 - \frac{\nu_f}{\nu_s} + \frac{\mathrm{h}\prime}{\nu_s}$ refer to as I' (h′). A linear function is obtained after converting, as shown in equation (11):

$$\frac{1}{E_t}\ \frac{1}{\left(1-\mathrm{e}^{-\nu_s/h'}\right)} = \mathrm{L}(\mathrm{h}') \approx \frac{1}{E_f'} + \frac{1}{E_s}\left(0.5 - \frac{\nu_f}{\nu_s} + \frac{\mathrm{h}\prime}{\nu_s}\right) \qquad (11)$$

A schematic representation is shown in figure 1.7:

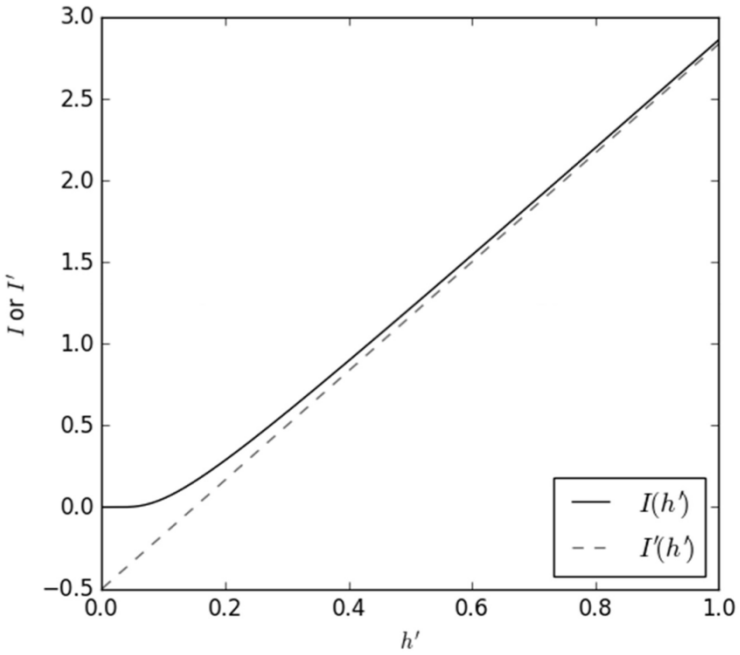

Figure 1.7 A schematic representation of function I and its asymptote I′. [16]

The slope of the function is $\frac{1}{E_s \nu_s}$, hence experiment data can be converted to a linear function and substrate modulus can be obtained from the slope of linear function.

Chapter 2

SAMPLES and METHODS

2.1 Mineral sample

Minerals are the main component of Earth's crust and mantle. Mineral properties such as elastic modulus are important for investigating the structure and properties of Earth. For our planet, the data we have on the Earth's interior are obtained from the measurement of seismic wave velocity. Measurement in laboratory of mineral's elastic properties are vital for the understanding of seismic information. Ten minerals are chosen to determine its elastic modulus: galena, beryl, calcite, dolomite, feldspar orthoclase, kyanite, microcline, obsidian and quartz. They are shown below:

Figure 2.1 Ten chosen mineral samples for this work.

Mineral samples are all natural grown and purchased from Scott Resource, Inc. Crystal system and chemical formula is shown in table 1.

Sample	Crystal system	Formula
Beryl	Hexagonal or Amorphous	$Be_3Al_2(SiO_3)_6$

Calcite	Trigonal	$CaCO_3$
Dolomite	Trigonal	$CaMg(CO_3)_2$
Feldspar orthoclase	Monoclinic	$KAlSi_3O_8$
Galena	Cubic	PbS
Kyanite	Triclinic	Al_2SiO_5
Microcline	Triclinic	$K(AlSi_3O_8)$
Obsidian	Amorphous	SiO_2
Quartz	Trigonal	SiO_2

Table 1 Crystal system and formula of sample.

2.2 Sample preparation

2.2.1 Preparation

The samples were first mounted by epoxy and irregular shape samples were cut using Struers Accutom-5 cutting machine, pictured in figure 2.2, cylinder shape samples with two horizontal surface was obtained.

Figure 2.2 Struers Accutom-5 cutting machine.

Grinding process was down by successive grade of diamond paper, from 200 grit to 600 grit. Followed by polish process which is completed by alumina suspension (0.3 μm, 0.5 μm, 1.0 μm), as shown in figure 2.3.

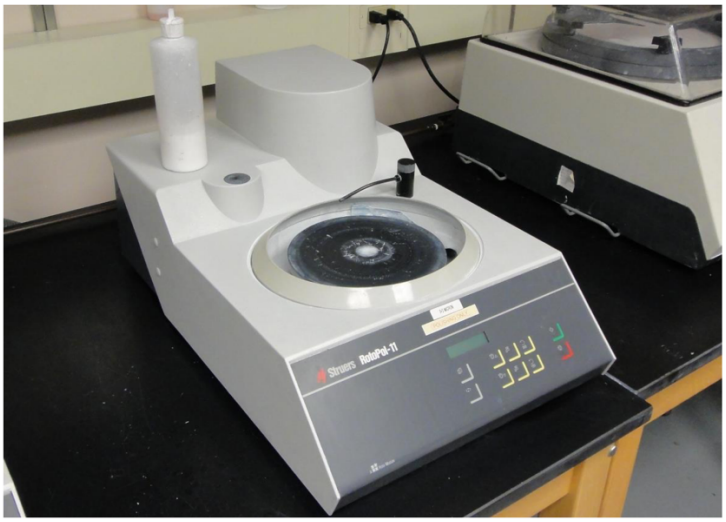

Figure 2.3 Struers RotoPol-11 Surface Polisher.

2.2.2 Metallic film deposition

In order to eliminate the effect of the form of crack and defects, a layer of chromium film is deposited on our mineral sample. This deposition work is done by Denton Discovery 18 sputtering system, and equipment is pictured in figure 2.4:

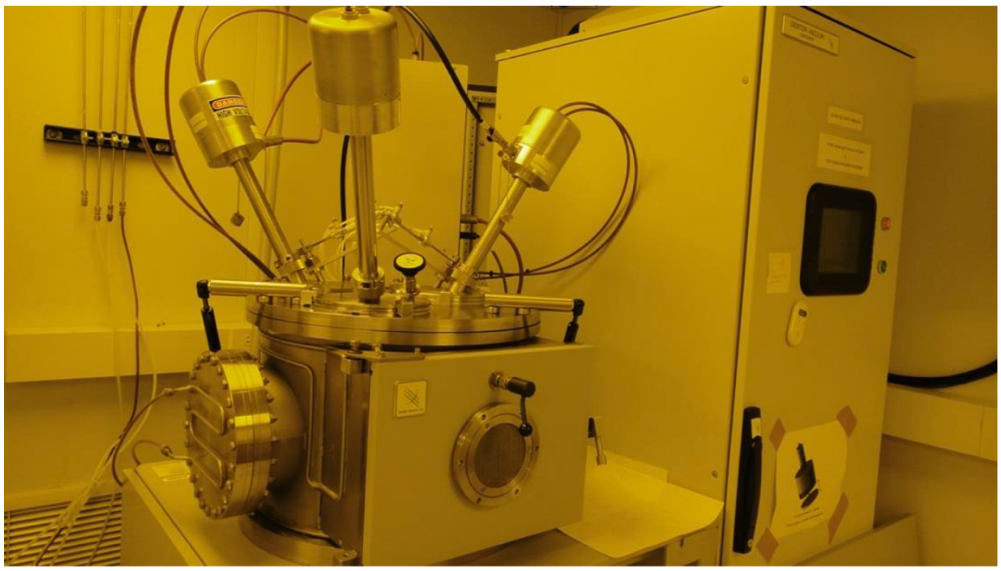

Figure 2.4 Denton Discovery 18 sputtering system.

All chromium film was deposited through Denton Discovery 18 sputtering system under DC power and substrate rotation. Before deposition, half of each mineral were covered by silicon wafer piece, therefore, only half of mineral was deposited with chromium. The purpose for this cover procedure is we could obtain both directly measured indentaion data of mineral and indentation data of mineral with chromium in one sample. Owing to the limitation of plate size inside the sputtering system, two batches of sample was deposited in same condition, nevertheless, film thickness may have little difference. Sputtering time was set as 1720 seconds and a 120 seconds pre-sputtering time was performed with closed target shutter in order to remove the contamination and oxidation on target. During the sputtering, sample holder was rotated to obtain uniform deposition. Detailed parameter is shown in table 2.

Sputtering power	DC
Target	Chromium
Pre-sputtering Power	200 W
Pre-sputtering time	120 s
Sputtering Power	200W
Sputtering time	1720 s
Gas 1 flow rate (Argon)	25 sccm
Deposition Temperature	Room Temperature
Ignition Pressure	80 mtorr
Expected film thickness	740 nm

Table 2 Chromium deposition parameters.

2.3 Experiment

2.3.1 Film thickness measurement

The film thickness of two batches of sample was measured by JEOL JSM 7000F scanning electron microscope (SEM). Equipment is picture in figure 2.5.

Figure 2.5 JEOL JSM 7000F scanning electron microscope.

Thickness was measured under second electron mode and back scattered mode in order to eliminate the edge effect. Film thickness on silicon wafer was measurement by SEM because silicon wafer is easier to operate under SEM. A sample of SEM images for film thickness measurement is shown in figure 2.6. Since even in same batch, film thickness varies in samples, the final thickness is the average of all measurement.

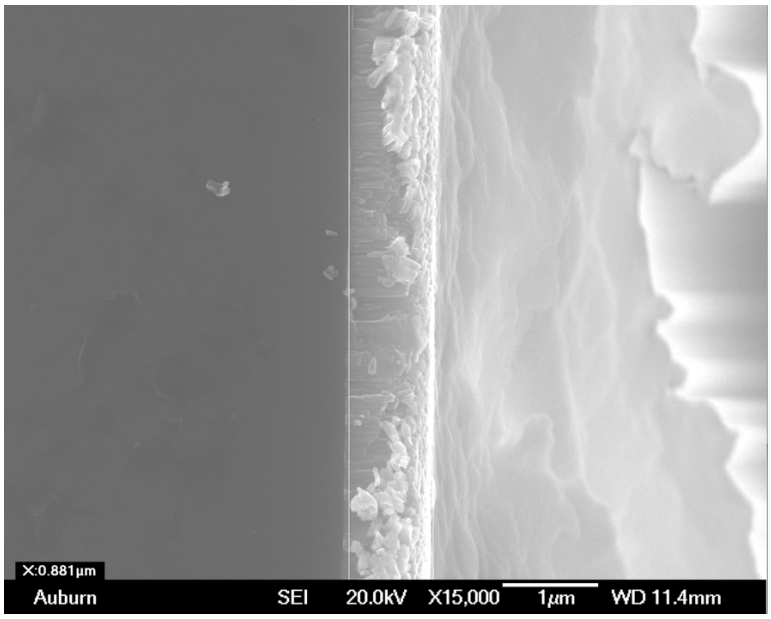

Figure 2.6 SEM image for film thickness measurement.

The measured film thickness of two batches sample are shown in table 3.

Sample	Film thickness (nm)
Beryl(Amorphous)	895
Calcite(104)	940
Dolomite(Polycrystalline)	895
Orthoclase(002)	940
Galena(200)	940
Kyanite(100)	940
Microcline(Microcrystalline)	895
Obsidian(Amorphous)	895
Quartz	895

Table 3 Film thickness measurement and X-Ray Diffraction result.

2.3.2 X-ray diffraction

Most of minerals are highly isotropic, hence, in order to identify crystal plane of mineral surface we test, X-ray diffraction was performed. Tested XRD results are compared with published results in database by utilizing PDFmaint and EVA. According to XRD results, single crystal and polycrystalline and amorphous, all exist in our sample, as shown in table 3 and figure 2.7.

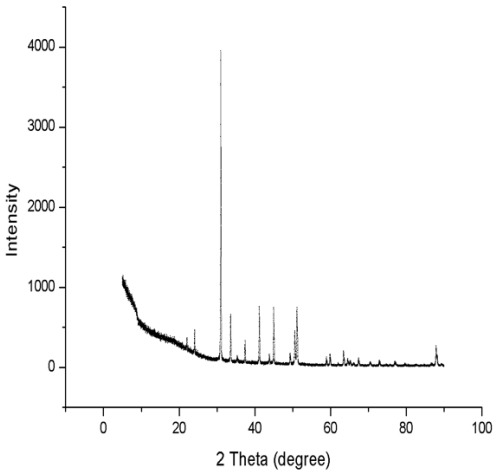

(a)

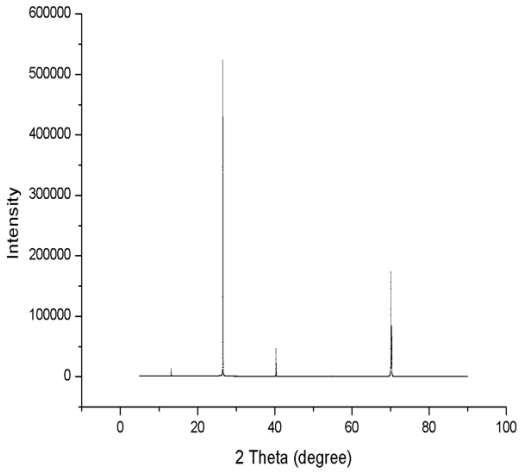

(b)

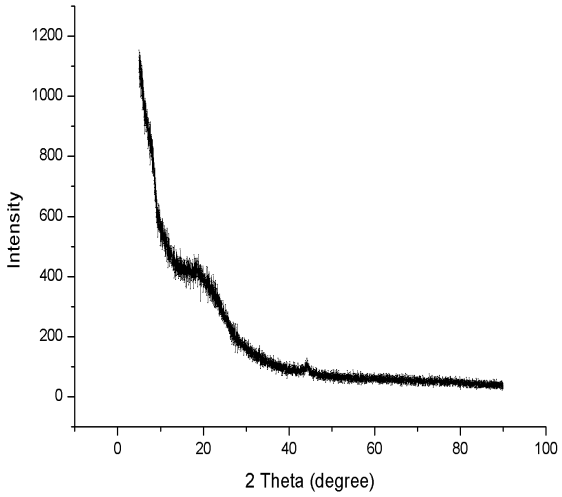

(c)

Figure 2.7 X-ray diffraction results for (a)dolomite (polycrystalline) (b)kyanite (singe crystal) (c) obsidian (amorphous).

2.3.3 Nanoindentation test

The modulus of minerals was obtained using MTS Nanoindenter XP with a Berkvoich diamond tip (three sided pyramid) under continuous stiffness method. For both direct measured mineral indentation data and mineral-chromium composite system indentation data, 5 × 5 arrays of indentation with 100 μm spacing was implemented. Testing frequency, harmonic displacement and thermal drift rate was set as 45 Hz, 2nm and 0.05 nm/s respectively. For our test, loading and unloading curve could be divided into four stages. At first, indenter tip is loaded and penetrates into sample with constant loading rate. Then, at peak load, it will hold for a short time. At third stage, unloading starts. Before end, indenter again hold for a short time, as least 50s, this is for correction of thermal drift which is caused by thermal expansion or thermal extraction in material [17].

Chapter 3

RESULTS and DISCUSSION

3.1 Indentation results SEM images of indents

As mentioned in chromium deposition part, half of mineral was covered by a piece of silicon wafer. Therefore, for each mineral sample, indentation test was performed on both mineral surface and chromium surface. An illustration of direct measurement and indirect measurement test area is shown in figure. Dark area in area A where a thin layer of gold was coated for SEM because some minerals in this work has bad electron conductivity. Gold coating region is where the indentation test was performed. Two main parts of results in this work, indentation results for all samples and SEM images of indents are shown in figure. For direct measurement results, y axis is elastic modulus and y axis is composite modulus for indirect measurement (film-substrate system) results. Penetration depth is equal to chromium film thickness of sample for both direct measurement and indirect measurement. This indicates that indenter will not penetrate into substrate and hence significantly reduce the risk of crack formation in minerals. For direct measurement results, the formation of crack is shown in SEM images of indents and pop in is observed in load curve. Both these two effects would lead to inaccurate elastic modulus and would be discussed in this chapter.

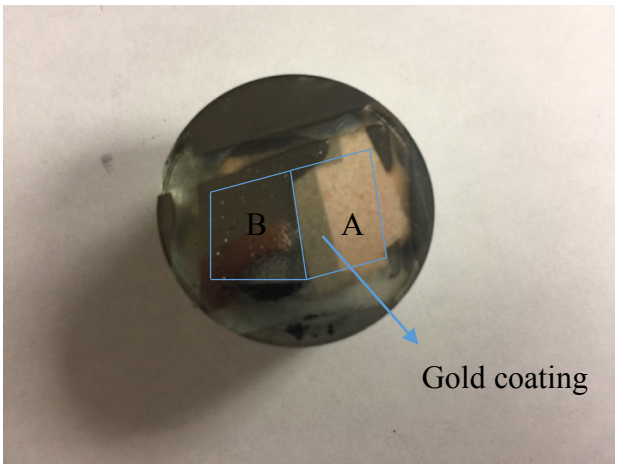

Figure 3.1 A illustration of indentation test area (A) direct indentation test (B) indirect indentation test.

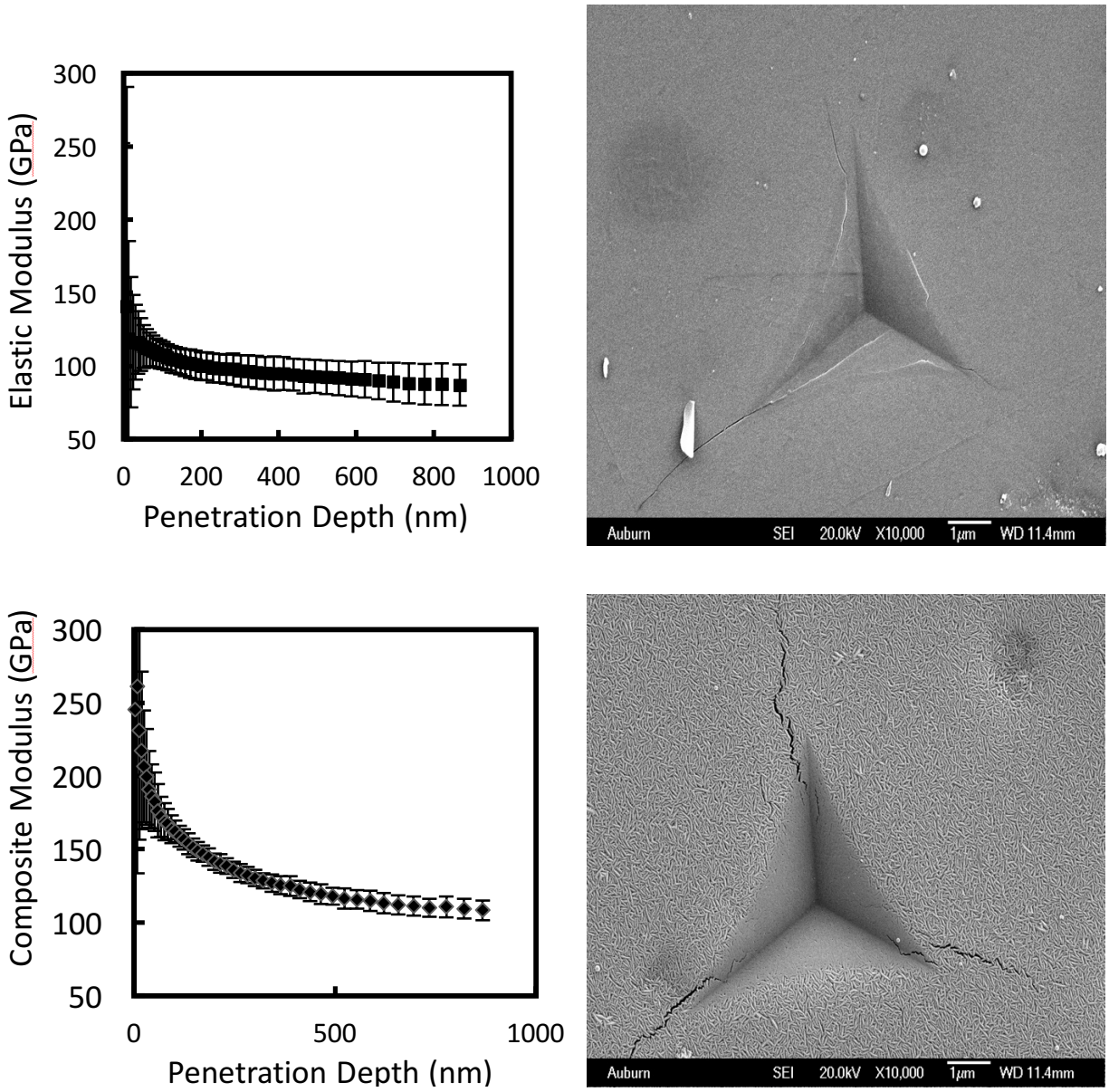

Figure 3.2 Quartz indentation test and SEM images result for direct and indirect measurement.

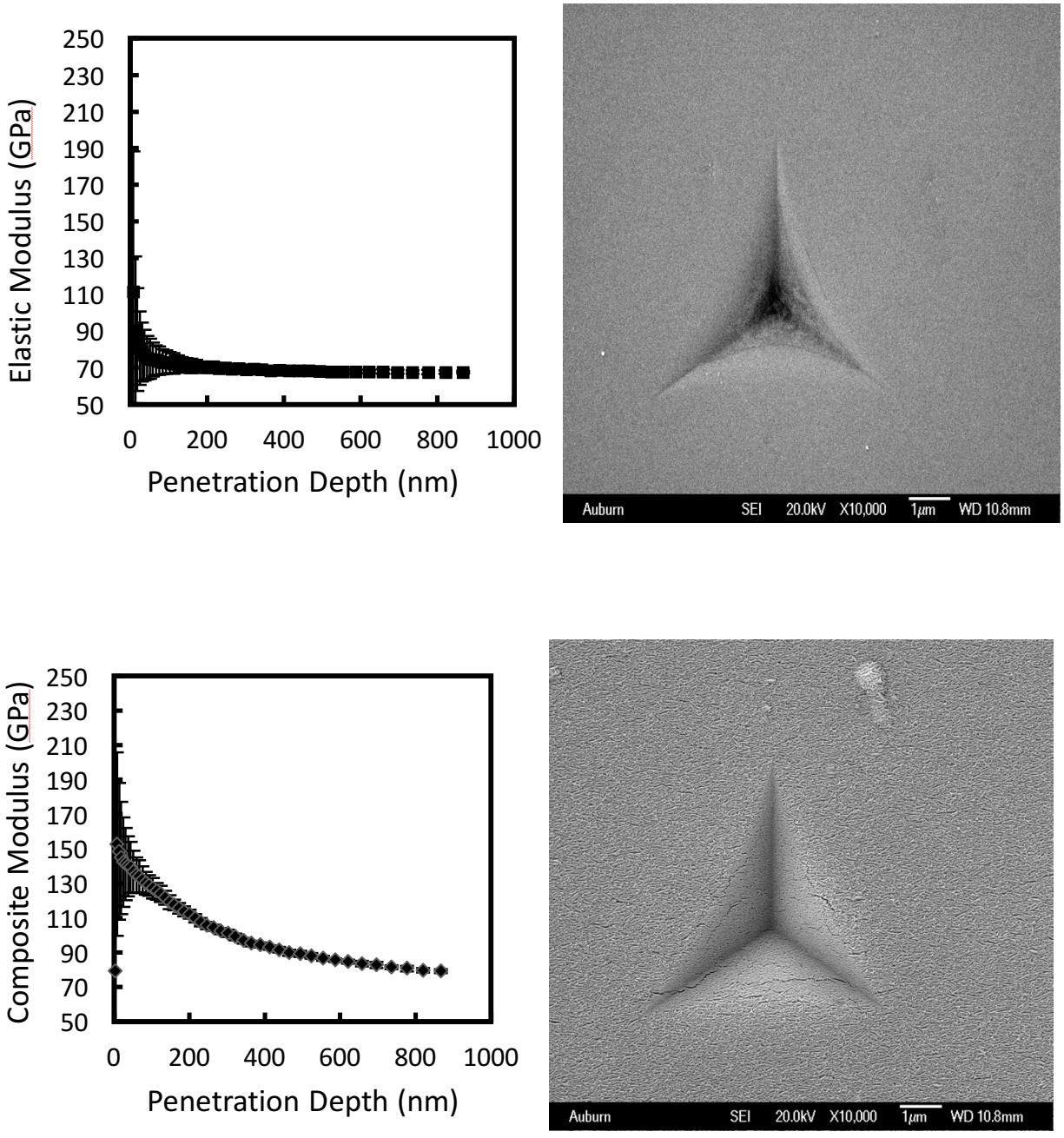

Figure 3.3 Obsidian indentation test and SEM images result for direct and indirect measurement.

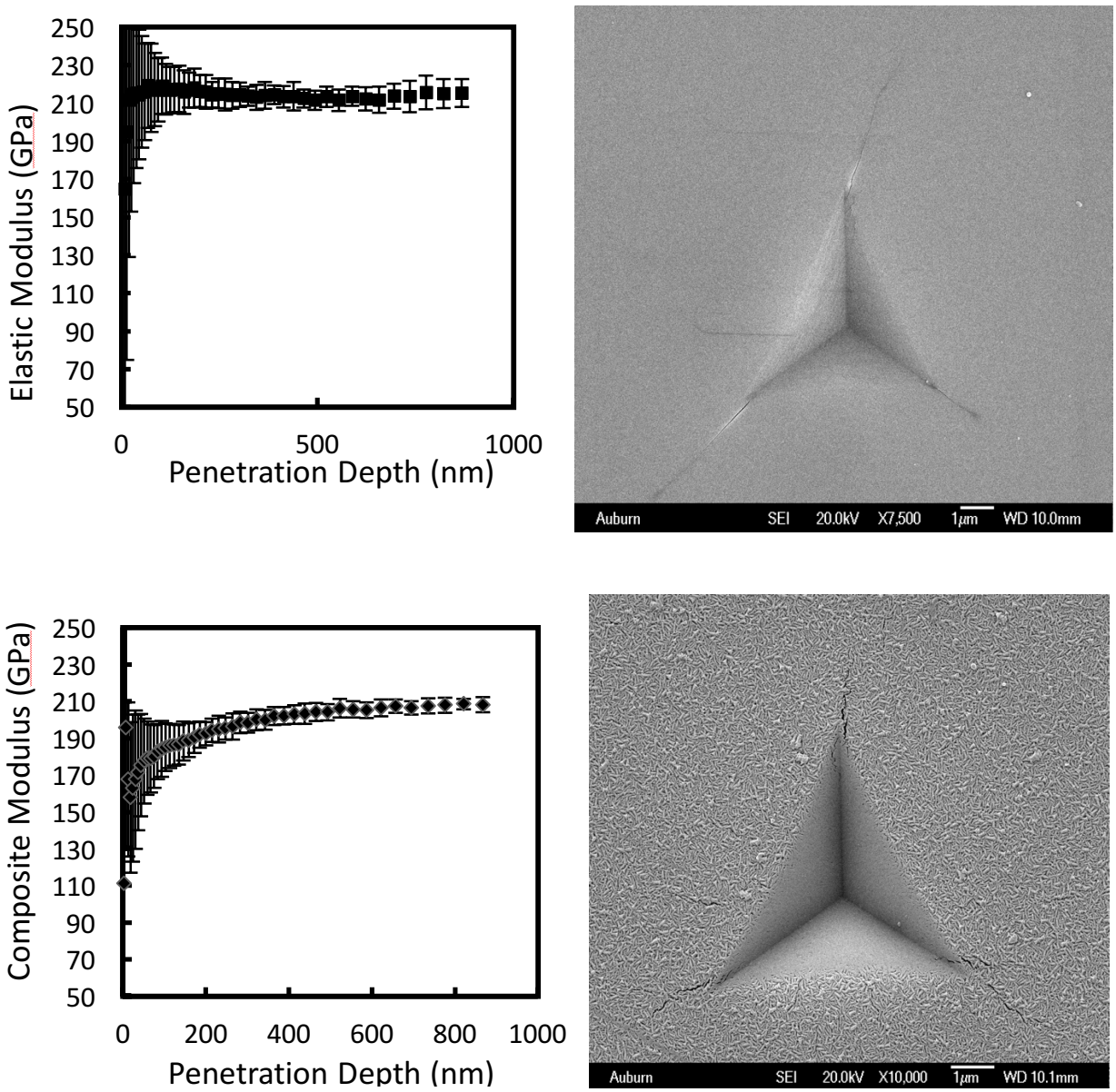

Figure 3.4 Beryl indentation test and SEM images result for direct and indirect measurement.

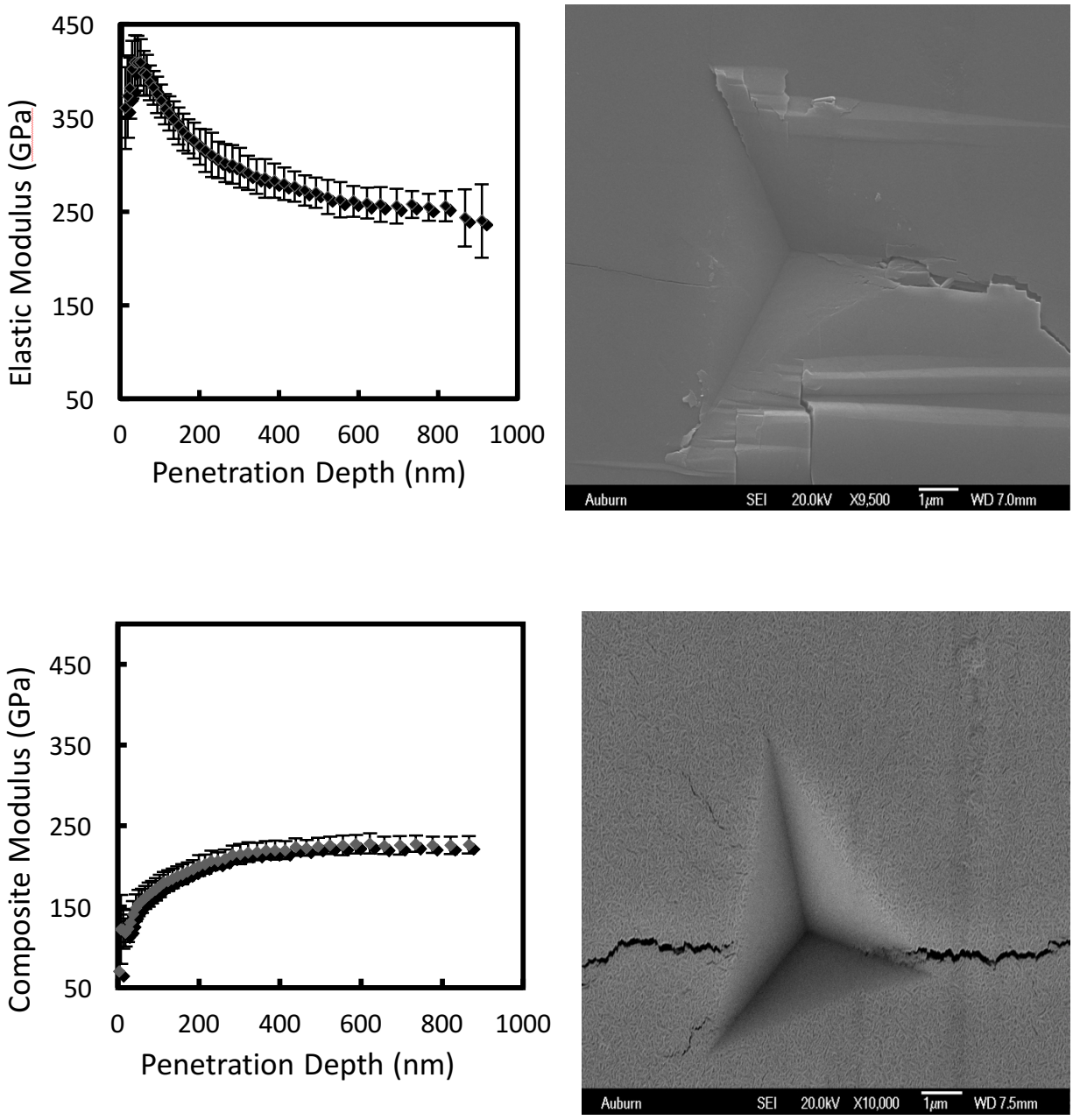

Figure 3.5 Kyanite indentation test and SEM images result for direct and indirect measurement.

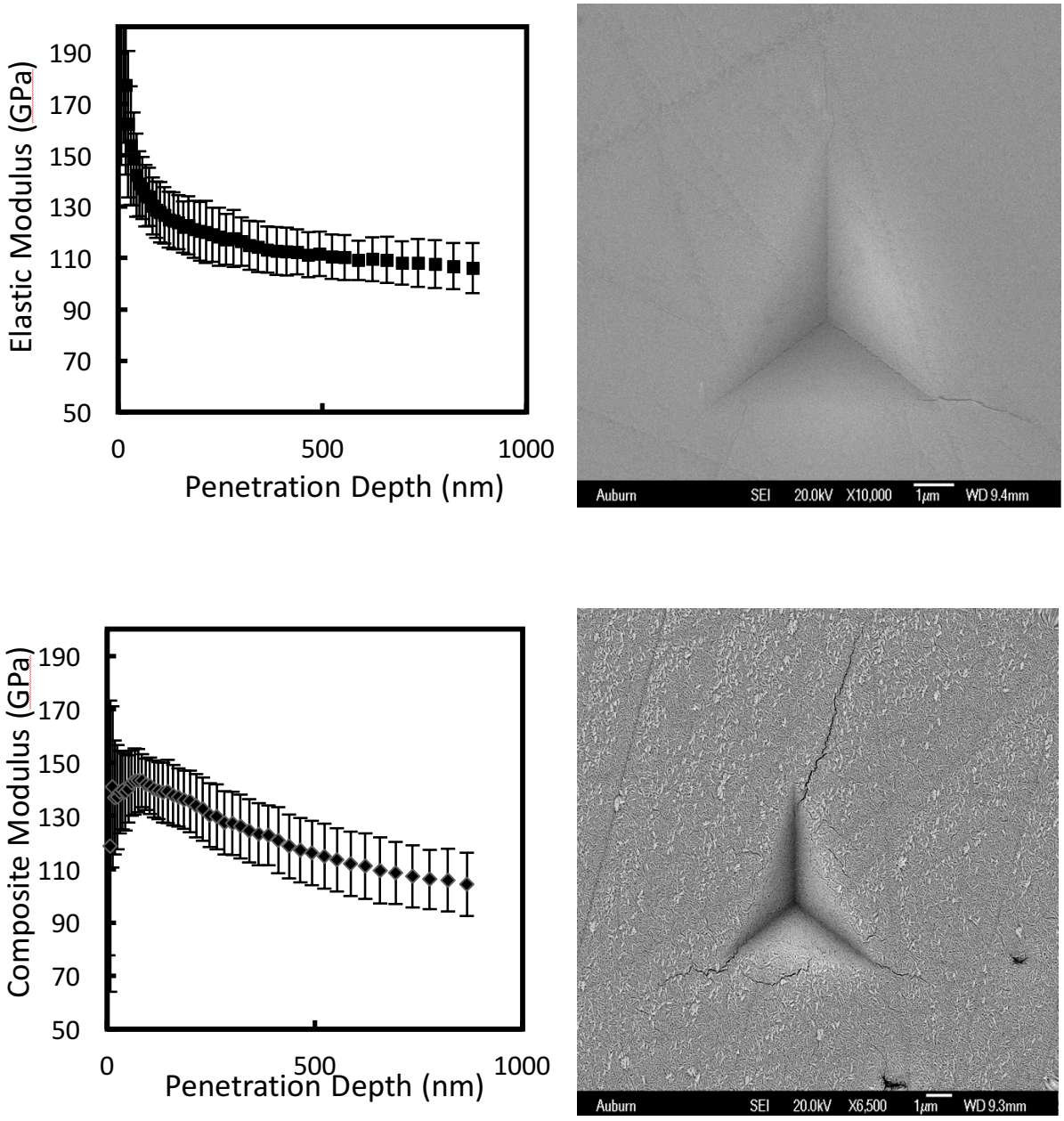

Figure 3.6 Dolomite indentation test and SEM images result for direct and indirect measurement.

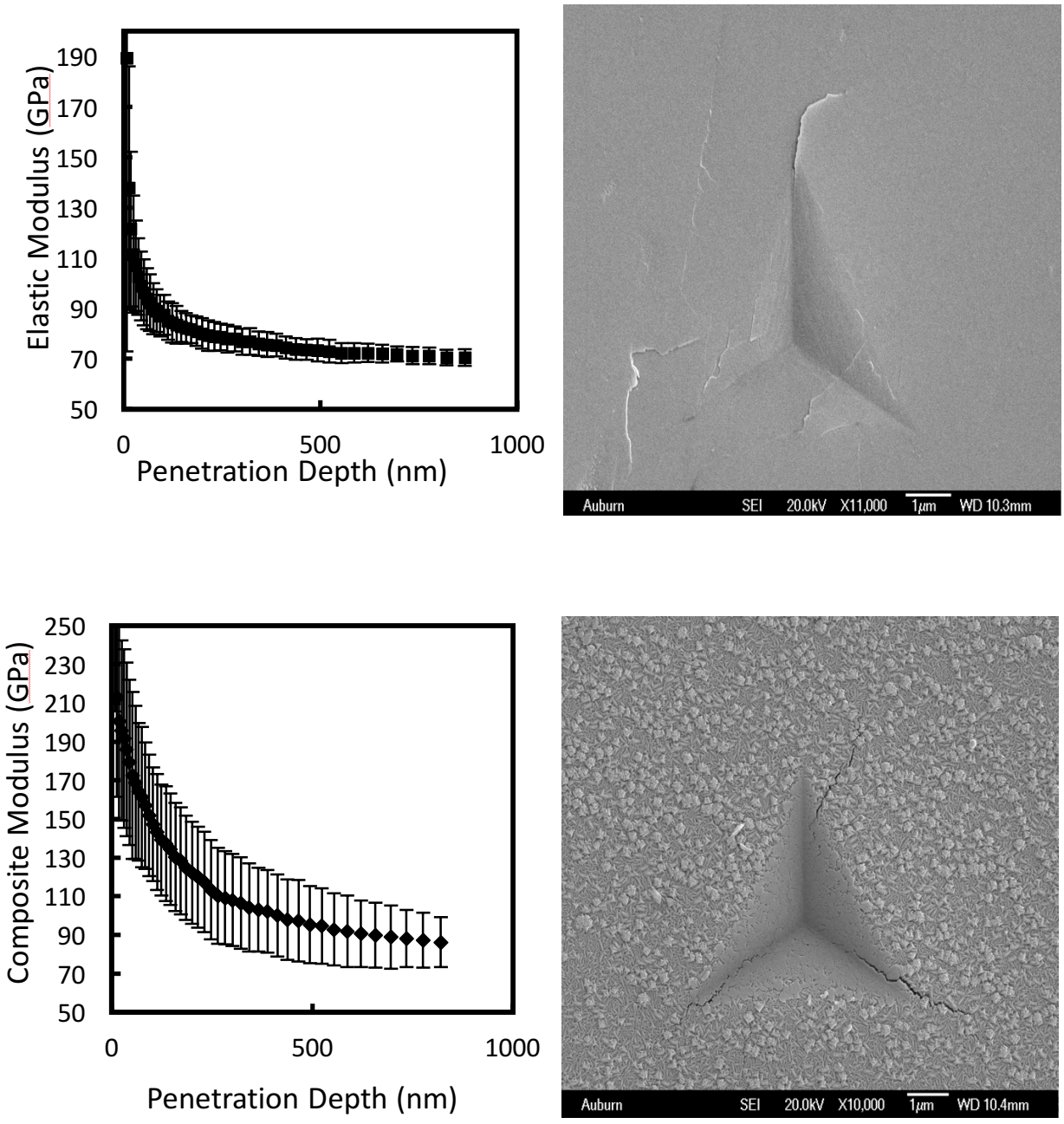

Figure 3.7 Microcline indentation test and SEM images result for direct and indirect measurement.

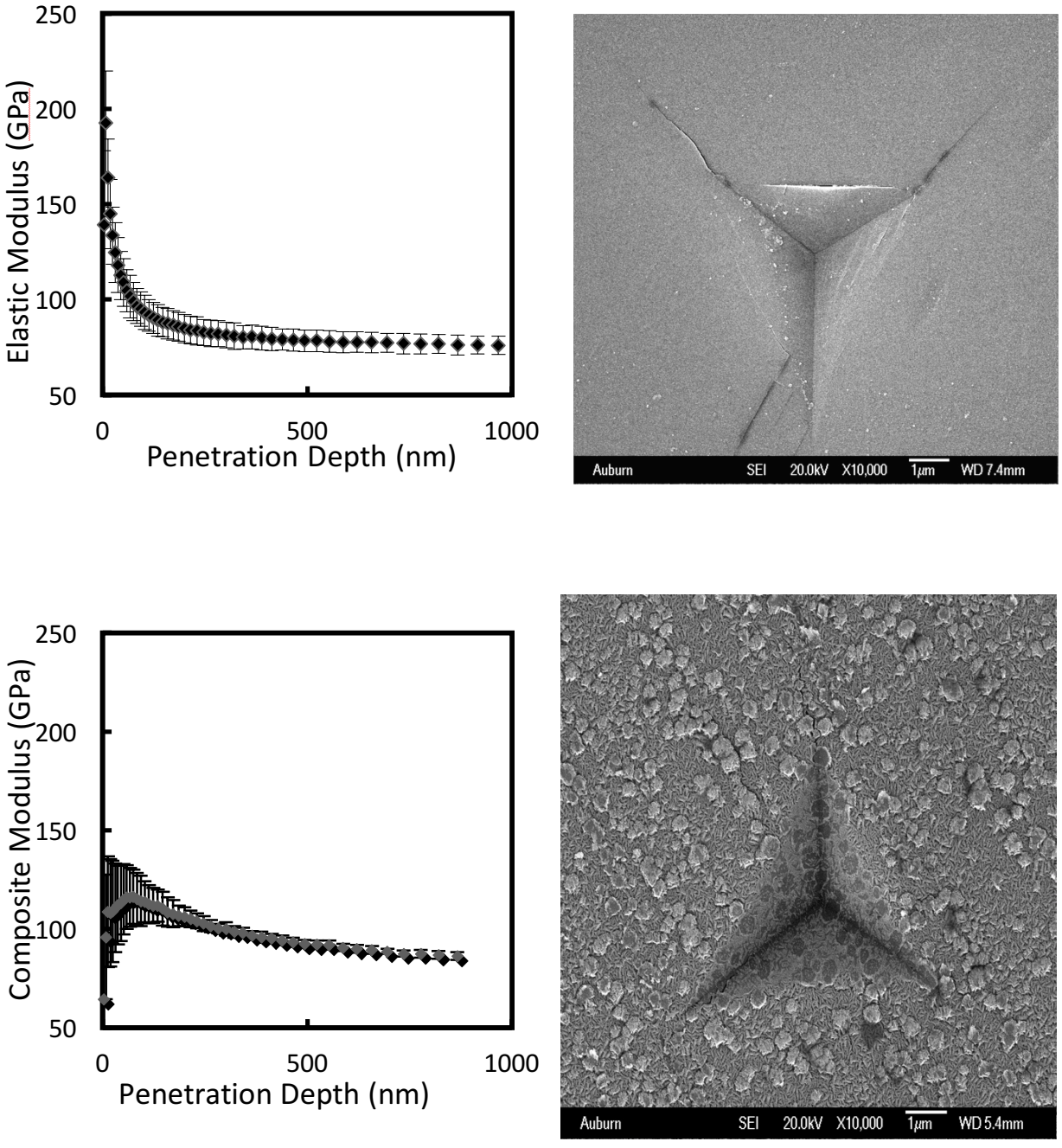

Figure 3.8 Feldspar orthoclase indentation test and SEM images result for direct and indirect measurement.

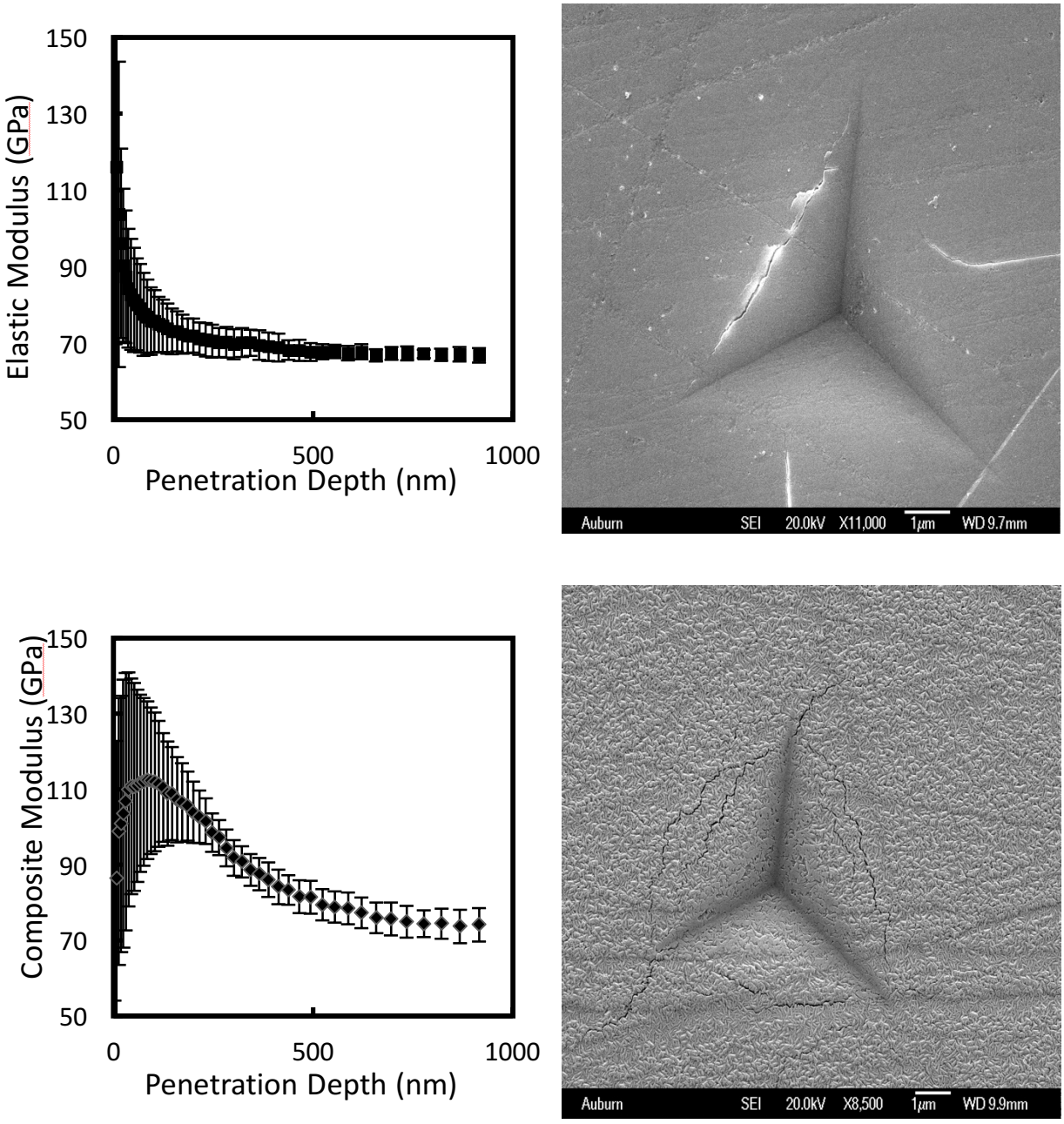

Figure 3.9 Calcite indentation test and SEM images result for direct and indirect measurement.

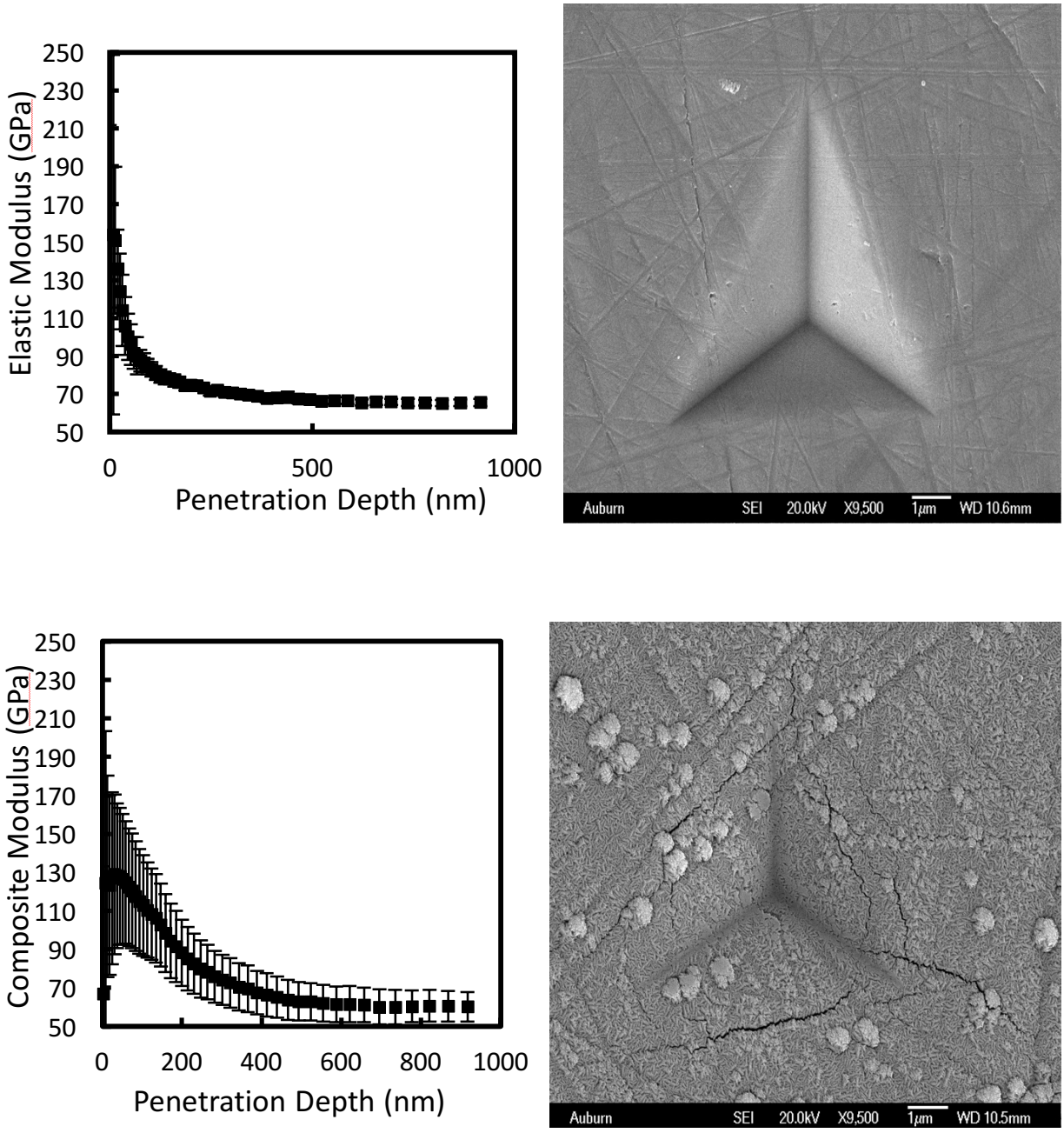

Figure 3.10 Galena indentation test and SEM images result for direct and indirect measurement.

It can be seen that in direct measured indentation result of quartz in figure 3.2, elastic modulus decreasing with penetration depth. The initial 20% of indentation data is not accurate due to the vibration of indenter tip and the contact between indenter tip and sample surface. This decreasing trend is the evidence of crack formation, it consumes elastic energy under loading and lead to

lower contact stiffness. Hence, based on equation (4), lower elastic modulus will be obtained. Cracks are obvious in SEM of indents on quartz, crack forms at three corners of indent, the reason is stress concentration at three corners are the highest. Results are similar for quartz, beryl, dolomite, microcline and orthoclase.

Composite modulus, which is the indentation test result of film substrate composite system, also decreases with penetration depth. Composite modulus is a mixture of film elastic modulus and substrate elastic modulus, at the beginning, composite modulus is dominated by film elastic modulus and as the indenter approaches to substrate, it starts to dominated by substrate. Quartz has lower elastic modulus than chromium, so composite modulus shows a downtrend. In this work, except beryl and kyanite, all other minerlas has lower elastic modulus than chromium.

For obsidian, as shown in figure 3.3, no obvious crack can be seen on indent. However, sink in is very noticeable, as mentioned in first chapter, sink in would cause smaller contact area and lead to underestimation of elastic modulus. By contrast, sink in was significantly minimized when indent on chromium with obsidian. Therefore, chromium film could significantly minimize the effect of sink in for obsidian. For kyanite (figure 3.5), results are a little different, cracks are very remarkable at indent on kyanite surface, and even some collapse can be observed. Also, cracks on indent at chromium surface is different, crack form at one corner of indent and corresponding perimeter. In order to investigate how this shape of crack forms, four indentation test with different penetration depth, from 200nm to 500nm, was performed on kyanite with chromium. SEM images was taken for each indents at different penetration depth, results are shown in figure.

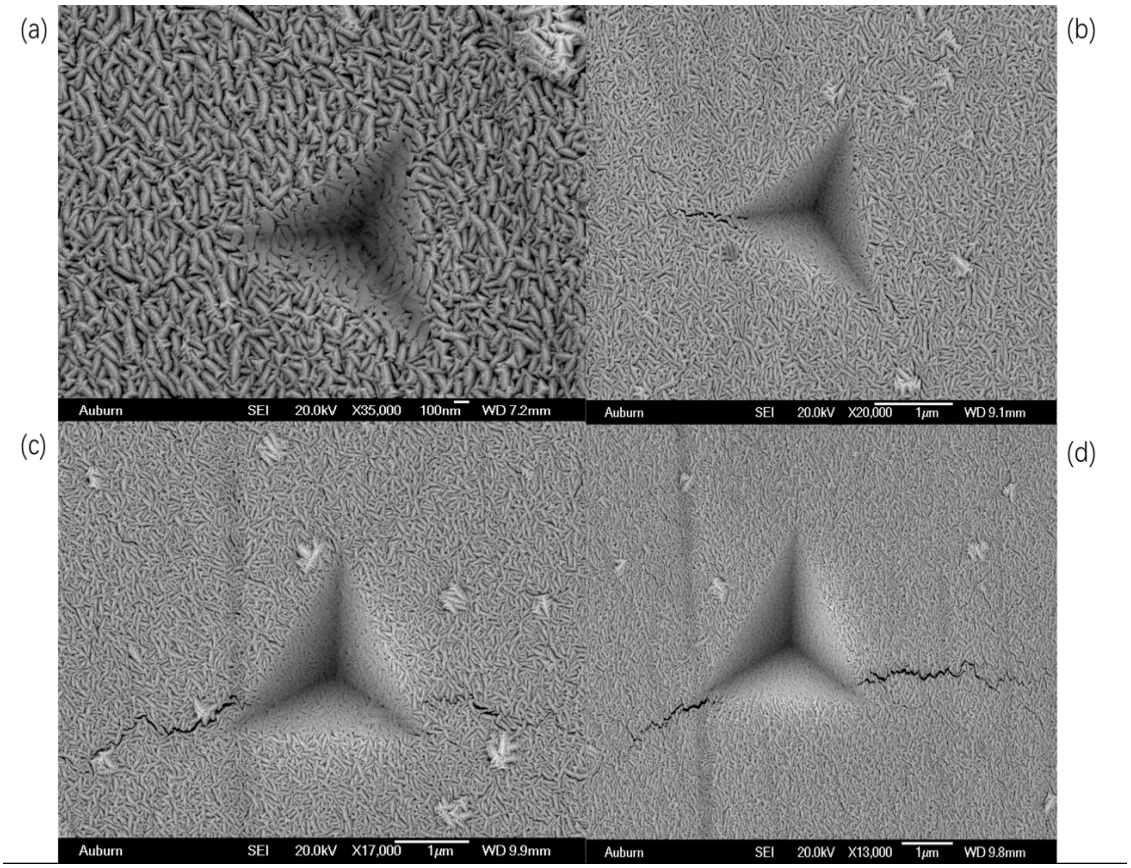

Figure 3.11 Indentation test for different penetration depth on chromium-kyanite composite system (a)200nm (b)300nm (c)400nm (d)500nm.

There is no obvious crack on 200nm penetration depth indent. A small crack is formed at one corner of indent at SEM image of 300nm penetration depth and crack forms at corresponding perimeter at 400 nm penetration depth. At SEM image of 500nm penetration depth, crack grows further. One possible reason is cleavage plane, which is at which plane, mineral tend to split along at this crystallographic structural plane. For kyanite, cleavage plane is (100) and (010) [18]. According to our X-ray diffraction result, the kyanite surface we tested is (100), therefore, cracks tend to form along (010).

An interesting phenomenon is a lot of particles could be observed on chromium surface at orthoclase, microcline and galena. In order to know what these particles are, high magnification SEM images of these particles are taken, as shown in figure.

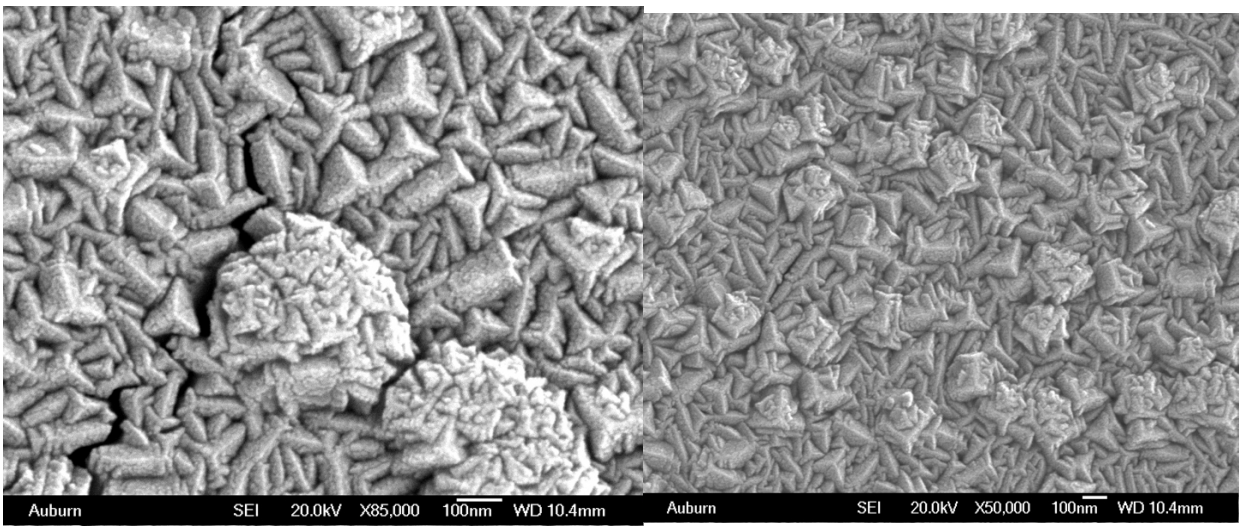

Figure 3.12 SEM images for particles on chromium with microcline

These particles are actually made of grains, hence, they are chromium. The reason is natural grown minerals has unsmooth surface as shown in figure. When depositing chromium, chromium tends to nucleate on those small holes. Consequently, a lots of particle formed on chromium surface.

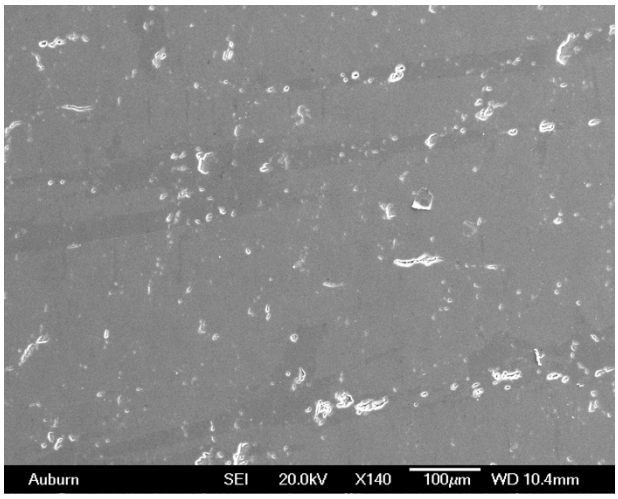

Figure 3.13 SEM image of microcline surface

Another different result shows on calcite and galena, as shown in figure 3.9 and 3.10, circle shape crack forms around indent edge on chromium instead of three cracks at corner. One explanation is low elastic modulus of calcite and galena, when indenter penetrates into surface, larger displacement at substrate than film, once crack formed on film, delimination occurs on film and lead to circle shape crack. In fact, elastic modulus of galena and calcite are the two lowest among nine minerals.

3.2 Pop in

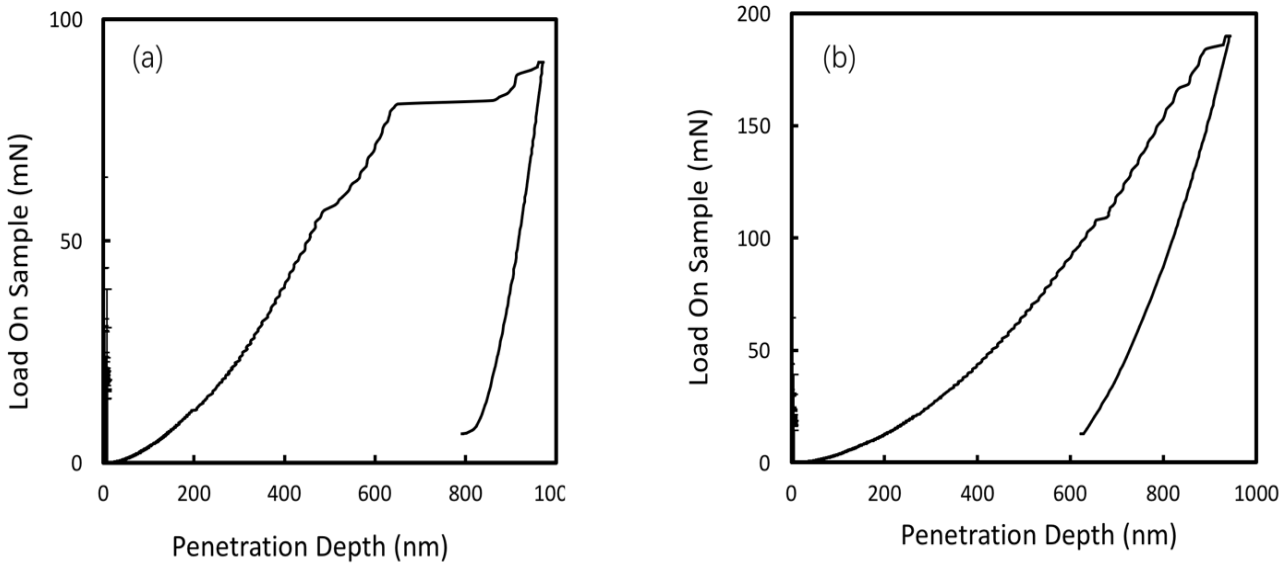

Figure 3.14 Pop-in observed in indentation test for kyanite (a) single pop-in (b) successive pop-in

Pop in was observed on direct indentation test result of kyanite, dolomite, quartz and beryl. Pop in means there are one or more displacement excursion on load curve. There are two types of pop in behavior, single pop-in which a large displacement excursion produced, and successive pop-in which several small displacement excursions produced. The layered structure of kyanite is one of the reason that very remarkable pop in was observed during indentation test. When cracks and defects forms during testing, they are easier to propagate along plane between two layers. Pop in was not observed in galena and calcite because their elastic modulus is too small, load was not high enough to support the occurrence of pop in. And for other three minerals, obsidian, microcline and orthoclase, the possible reason could be their structure. Work done by Yuzhi Xia, Yanfei Gao and George M.Pharr [19]shows that pop in is related with indenter tip radius, homogeneous and heterogeneous dislocation nucleation. Moreover, first pop in is determined by homogeneous dislocation and type of pop in depends on material. As for the influence of pop-in on elastic modulus, when pop-in occurs, load-displacement curve will deviate from original path and change the slope of unloading curve. In contrast, as shown in figure, a perfect load curve was obtained, pop in was not observed and also for all other mineral with chromium composite. Therefore, chromium film could eliminate the effect of pop in.

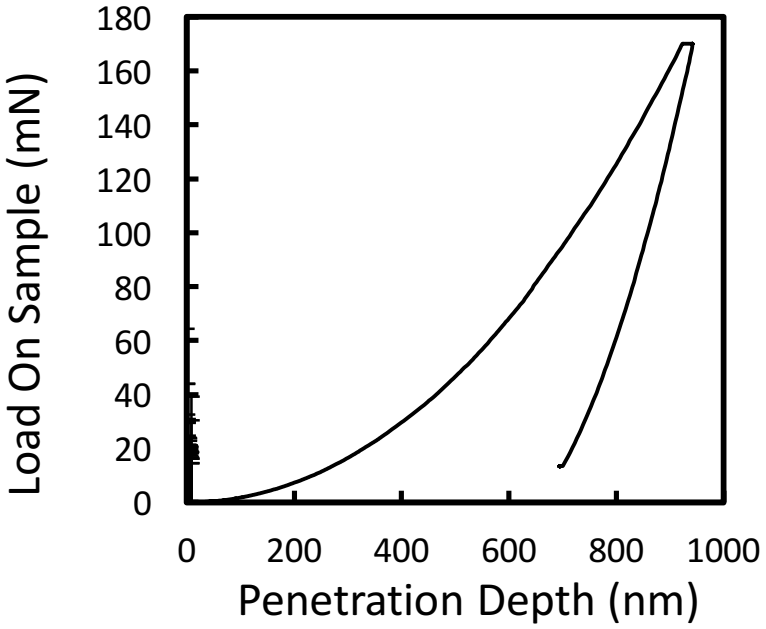

Figure 3.15 Load versus displacement for indirect indentation test on chromium with kyanite

Other aspects that may influence the result of direct indentation test like surface roughness of sample, when indent on valley region, higher elastic modulus would be obtained, and lower modulus would be obtained if indent on crest region. This condition is similar with pile-up and sin-in. Deposited chromium film has more smooth surface than natural grown minerals.

3.3 Zhou-Prorok model and Chen-Prorok method results

All calculation results for Zhou-Prorok model and Chen-Prorok method are shown in table.

Sample	Poisson's ratio	Modulus (Literature value)	Z-P model result (GPa)	Chen-Prorok method result (GPa)
Beryl(Amorphous)	0.039[20]		168	214
Calcite(104)	0.322[21]	72-88[26]	65	64
Dolomite(Polycrystalline)	0.2[22]	53-82[27]	90	93

Orthoclase(002)	0.29[23]	89±7[28]	75	79
Galena(200)	0.27[24]		49	55
Kyanite(100)	0.24[25]	227±30[28]	222	237
Microcline(Polycrystalline)	0.245[23]	69[30]	75	74
Obsidian(Amorphous)	0.185[24]	68[29]	68.5	69
Quartz	0.075[23]	117±3[28]	87	98

Table 4 Substrate information and calculated results for all minerals

The source of deviation in both Zhou-Prorok model and Chen-Prorok method could be compared. For Zhou-Prorok model, we need to know film thickness, Poisson's ratio of film and substrate, film modulus, then substrate modulus could be obtained by fitting with experiment data. From Yan's method, it has shown that once the slope ($\frac{1}{E_S \nu_s}$) is obtained, the effect of substrate Poisson's ratio (ν_s) could be cancelled out. The influence of Poisson has been discussed in Yan's paper and demonstrated that the lower the film Poisson's ratio, the more superposition between I(h′) and I′(h′). Eventually, chromium was chosen as the best film to extract substrate modulus from film substrate system, as shown in figure.

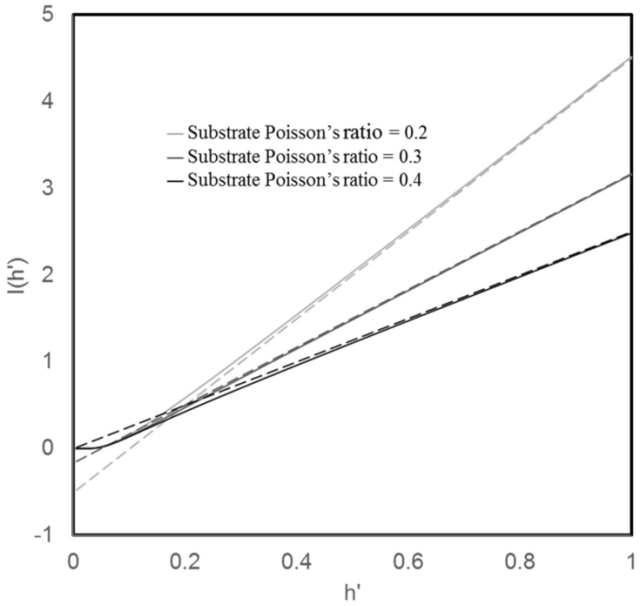

Figure 3.16 I(h′) and I(h′) function with chromium film for different substrate Poisson's ratio. [15]

Therefore, as long as we have a rough estimate of film thickness, elastic modulus of substrate could be extracted from film-substrate system. The most possible deviation for Chen-Prorok method is the approximated linear function. According to figure, this deviation is limited. For Zhou-Prorok model, the deviation could come from several aspects, for example, nonuniform deposition, measurement of film thickness, film properties, etc. Consequently, Chen-Prorok method result is more recommended for the substrate modulus. Figure 3.17 shows indentation test result, Zhou-Prorok model, L(h') function of calcite and dolomite in one graph.

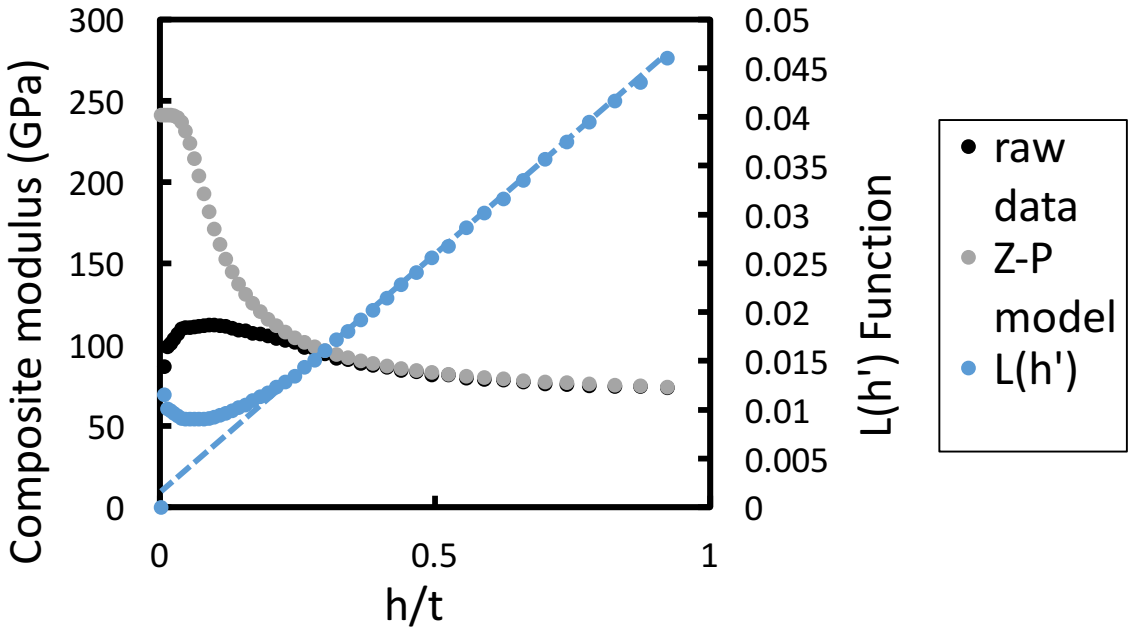

(a)

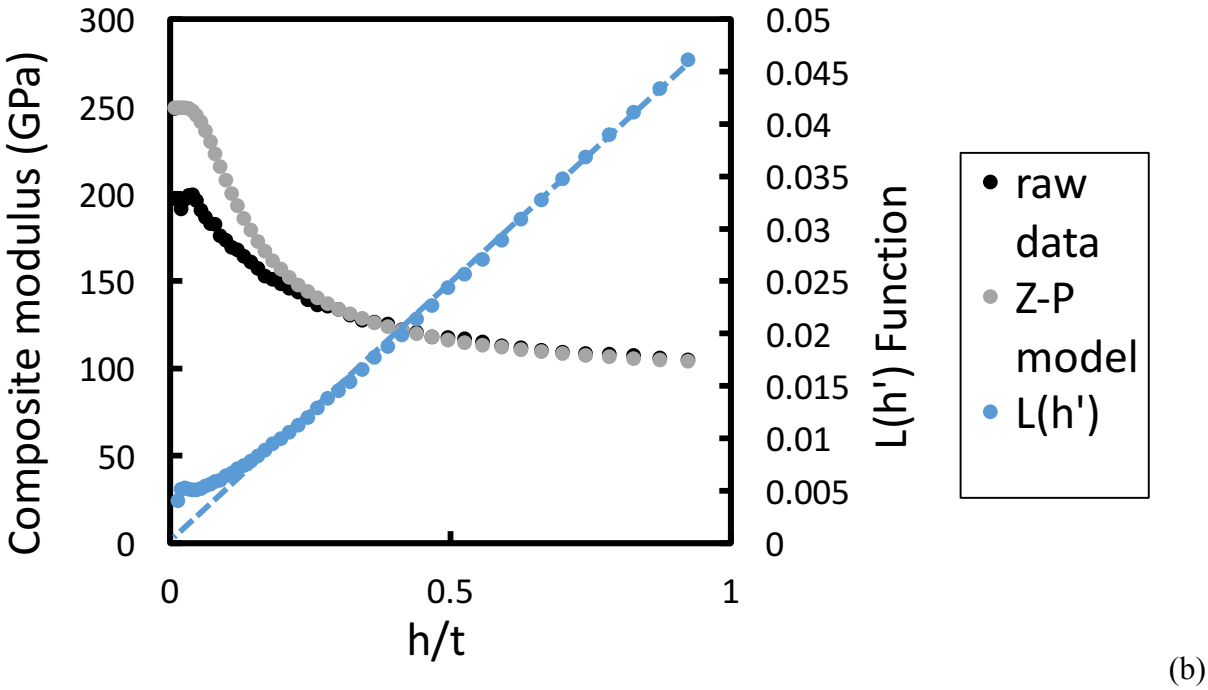

(b)

Figure 3.17 Indentation test result, Zhou-Prorok model, L(h') function of (a) Calcite and (b)Dolomite

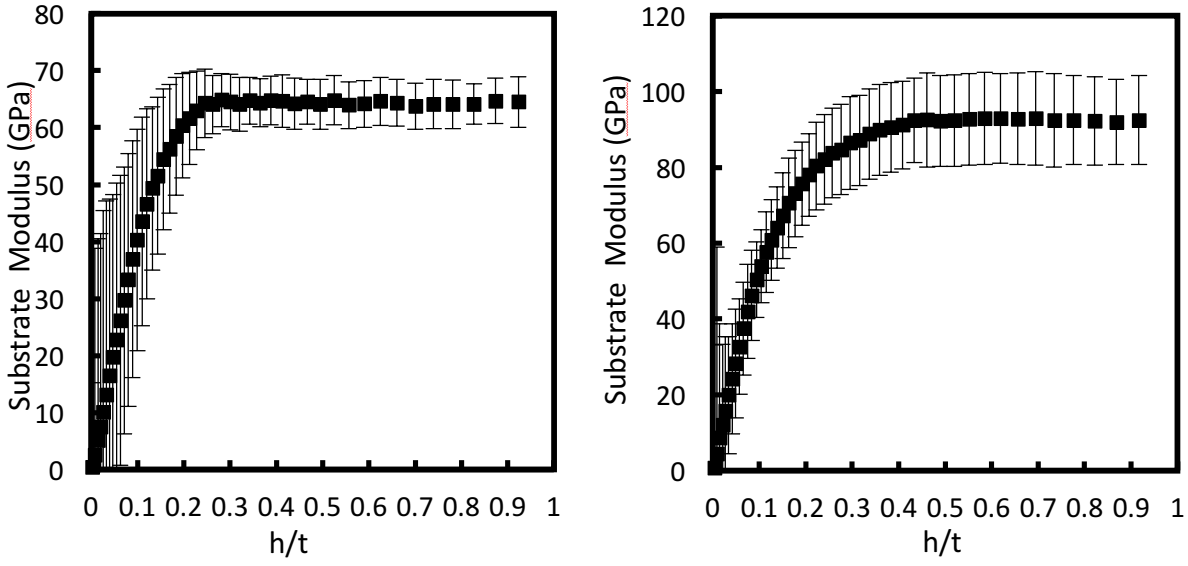

(a) (b)

Figure 3.18 Chen-Prorok method results of (a) Calcite and (b)Dolomite

h/t is reduced displacement and h is displacement and t is film thickness. L(h') become linear quicker than Zhou-Prorok model match raw data, this is also an evidence that Chen-Prorok method could obtain more accurate elastic modulus. From the slope of L(h') function, we could obtain the value of substrate modulus as shown in figure 3.18. A flat region occurs after 0.3 (h/t) for calcite and 0.5 (h/t) for dolomite. Therefore, we could get a stable result for substrate modulus. The start point of raw data should be close to the modulus of film, which is 279 GPa (modulus of chromium). For almost all sample's experiment results, the modulus starts from around 150 GPa, this is unexpected. One possible reason for that is sink-in, sink-in was observed with varying extent in all SEM images of indent on chromium-mineral composite system. Since, compared to chromium, all minerals we chosen are more compliant chromium. Therefore, as mentioned in chapter 1, for film-substrate composite system, when substrate is more compliant than film, sink in occurs. Actual contact is smaller than expected, hence, according to equation (4), lower elastic modulus will be obtained.

Chapter 4

CONCLUSION

In this work, elastic modulus of nine minerals are obtained from indirect indentation test. Unlike traditional indentation test, which is directly indent on mineral surface and cause crack formation and pop in, both result in inaccurate elastic modulus. Crack could assume elastic energy and lead to lower elastic modulus, pop in could cause deviation on load curve also affect the result of elastic modulus. A more reliable and accurate way to determine elastic modulus is performed in this work, a layer of chromium was deposited on mineral surface, and eliminate the effect of pop in, moreover, highly reduce the risk of crack formation in minerals. Focused ion beam (FIB) test could be done in future for a stronger proof of no crack in mineral. By comparing the deviation from Zhou-Prorok model and Chen-Prorok method, also, based on graphs, it can be concluded that Chen-Prorok method is a better way to determine elastic modulus of minerals. Cleavage plane may influence the crack formation on chromium with kyanite. Chromium nucleation was observed on microcline, orthoclase and galena due to their unsmooth surface. Effect of nucleated chromium on chromium surface for indentation test haven't been investigated.

REFERENCES

[1] Li, X., & Bhushan, B. (2002). A review of nanoindentation continuous stiffness measurement technique and its applications. *Materials characterization*, *48*(1), 11-36.

[2] Oliver, W. C., & Pharr, G. M. (1992). An improved technique for determining hardness and elastic modulus using load and displacement sensing indentation experiments. *Journal of materials research*, *7*(06), 1564-1583.

[3] Sneddon, I. N. (1965). The relation between load and penetration in the axisymmetric Boussinesq problem for a punch of arbitrary profile. *International journal of engineering science*, *3*(1), 47-57.

[4] Oliver, W. C., & Pharr, G. M. (2004). Measurement of hardness and elastic modulus by instrumented indentation: Advances in understanding and refinements to methodology. *Journal of materials research*, *19*(01), 3-20.

[5] MariAnne Sullivan , Doctor's dissertation, Materials Engineering, Auburn, Fall 2015.

[6] Li, X., & Bhushan, B. (2002). A review of nanoindentation continuous stiffness measurement technique and its applications. *Materials characterization*, *48*(1), 11-36.

[7] Li, J., & Chou, T. W. (1997). Elastic field of a thin-film/substrate system under an axisymmetric loading. *International Journal of Solids and Structures*, *34*(35-36), 4463-4478.

[8] Huajian, G., Cheng-Hsin, C., & Jin, L. (1992). Elastic contact versus indentation modeling of multi-layered materials. *International journal of Solids and Structures*, *29*(20), 2471-2492.

[9] Tsui, T. Y., & Pharr, G. M. (1999). Substrate effects on nanoindentation mechanical property measurement of soft films on hard substrates. *Journal of Materials Research*, *14*(01), 292-301.

[10] Bückle, H. (1973). Use of the hardness test to determine other material properties. *The Science of Hardness Testing and Its Research Applications*, 453.

[11] Zhou, B., & Prorok, B. C. (2010). A discontinuous elastic interface transfer model of thin film nanoindentation. *Experimental Mechanics*, *50*(6), 793-801.

[12] Doerner, M. F., & Nix, W. D. (1986). A method for interpreting the data from depth-sensing indentation instruments. *Journal of Materials research*, *1*(04), 601-609.

[13] Zhou, B., & Prorok, B. C. (2010). A new paradigm in thin film indentation. *Journal of Materials Research*, *25*(09), 1671-1678.

[14] Huajian, G., Cheng-Hsin, C., & Jin, L. (1992). Elastic contact versus indentation modeling of multi-layered materials. *International journal of Solids and Structures*, *29*(20), 2471-2492.

[15] Yan Chen, Master's thesis, Materials Engineering, Auburn, Summer 2016.

[16] Hazewinkel, M. (2001). Hyperbolic functions, Encyclopedia of Mathematics.

[17] MTS System corporation,"Theory of Instrumented Indentation Testing (IIT),"pp.38,2002

[18] Webster, R. (1962). Gems; Their sources, descriptions and identification.

[19] Xia, Y., Gao, Y., Pharr, G. M., & Bei, H. (2016). Single versus successive pop-in modes in nanoindentation tests of single crystals. *Journal of Materials Research*, *31*(14), 2065-2075.

[20] Cardarelli, F. (2008). *Materials handbook: a concise desktop reference*. Springer Science & Business Media.

[21] Lin, C. C. (2013). Elasticity of calcite: thermal evolution. *Physics and Chemistry of Minerals*, *40*(2), 157-166.

[22] Grady, D. E., Murri, W. J., & Mahrer, K. D. (1976). Shock compression of dolomite. *Journal of Geophysical Research*, *81*(5), 889-893.

[23] Nikolas I. Christensen. (1996)Poisson's ratio and crustal seismology. JOURNAL OF GEOPHYSICAL RESEARCH, 3139-3156

[24] Gercek, H. (2007). Poisson's ratio values for rocks. *International Journal of Rock Mechanics and Mining Sciences*, *44*(1), 1-13.

[25] Mikowski, A., Soares, P., Wypych, F., & Lepienski, C. M. (2008). Fracture toughness, hardness, and elastic modulus of kyanite investigated by a depth-sensing indentation technique. *American Mineralogist*, *93*(5-6), 844-852.

[26] Private Communication. J.A.Elliott. Dept. (2011). Materials Science, University of Cambridge.

[27] Viktorov, S., Golovin, Y., Kochanov, A., Tyurin, A., Shuklinov, A., Shuvarin, I., & Pirozhkova, T. (2014). Micro-and nano-indentation approach to strength and deformation characteristics of minerals. *Journal of Mining Science*, *50*(4).

[28] Whitney, D. L., Broz, M., & Cook, R. F. (2007). Hardness, toughness, and modulus of some common metamorphic minerals. *American Mineralogist*, *92*(2-3), 281-288.

[29] Syono, Y., & Manghnani, M. H. (1992). *High-pressure research: application to earth and planetary sciences* (Vol. 3). American Geophysical Union.

[30] Zhou, H., Liu, H., Hu, D., Yang, F., Lu, J., & Zhang, F. (2016). Anisotropies in Mechanical Behaviour, Thermal Expansion and P-Wave Velocity of Sandstone with Bedding Planes. *Rock Mechanics and Rock Engineering*, *49*(11), 4497-4504.